Numerical model for light propagation and light intensity distribution inside coated fused silica capillaries

Tomasz Piasecki ,MirekMacka , BrettPaull , DermotBrabazon

Abstract

Numerical simulations of light propagation through capillaries have been reported to a limited extent in the literature for uses such as flow-cell design. These have been restricted to prediction of light path for very specific cases to date. In this paper, a new numerical model of light propagation through multi-walled cylindrical systems, to represent coated and uncoated capillaries is presented. This model allows for light ray paths and light intensity distribution within the capillary to be predicted. Macro-scale (using PMMA and PC cylinders) and micro-scale (using PTFE coated fused silica capillaries) experiments were conducted to validate the model's accuracy. These experimental validations have shown encouragingly good agreement between theoretical predictions and measured results, which could allow for optimisation of associated regions for monolith synthesis and use in fluidic chromatography, optical detection systems and flow cells for capillary electrophoresis and flow injection analysis.

Keywords: Light propagation Light intensity Modelling Capillary Optical detection

1. Introduction

Organic monolithic stationary phases, since their first appearance in 1992, are considered one of the milestones in chromatography [1,2]. Several methods of monolith polymerisation initiation have been reported to date including by application of resistance heating, UV-irradiation, microwaves, electron beam and 7-radiation [3-6]. Photoinitiatedpolymerisation for monolith formation was successfully demonstrated for the first time in 1997 by Viklund et al. [3]. From all of these methods, heat and UV-irradiation are the most popular [7]. Better spatial control of monolith formation is possible with photoinitiatedpolymerisation than other techniques including thermal polymerisation. Recently it has been demonstrated that Light Emitting Diodes (LEDs) with wavelengths in the UV and visible region can be used as light sources for successful photoinitiatedpolymerisation of monoliths [7-9]. LEDs are an interesting alternative to traditional (incandescent and fluorescent) light sources having low cost, long life and unique spectral properties. Typical vessels for monoliths are fused silica capillary based microfluidic chips.

Whenever light is incident on the boundary of two transparent dielectrics, part of it is reflected and part is transmitted, see Fig. 1.

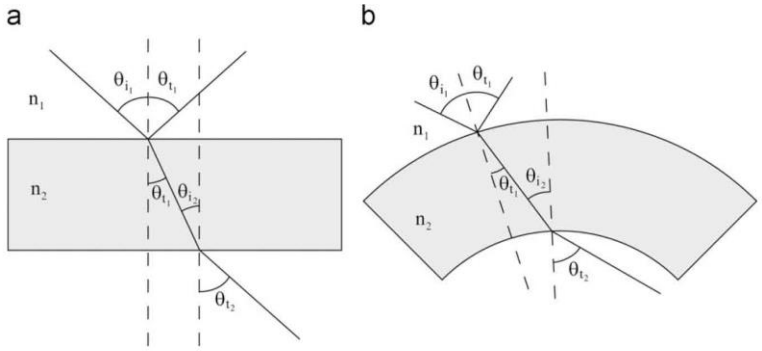

Fig. 1. Schematic of light transmission through: (a) a flat transparent material and (b) a cylindrical capillary, showing how curvature affects angle of incidence and transmittance.

Angle of incidence is related with angle of transmittance by Snell's Law (Eq. (1)). In the case of cylindrical symmetry, as in capillaries, it is possible that the exiting ray will not be parallel with the incident, see Fig. 1.

$$n_i \sin \theta_i = n_t \sin \theta_t$$

where n_i is the refractive index of the incident ray transmission medium, θ_i is the angle between incident wavevector and the normal to surface, n_t is the refractive index of the material through which the transmitted ray passes and θ_t is the angle between transmitted wavevector and normal to the surface. Light attenuation inside the absorbing medium is governed by the Lambert-Beer law (Eq. (2)).

$$I = I_o e^{-\alpha c l}$$

Where I is the light intensity at position I, which represents distance of passage through the medium, I_o is the initial light intensity, e is the Euler's number, α is the molar absorbance coefficient and c is the molar concentration.

Numerical modelling of physical processes has become more popular as computing power, that is readily available, has increased in recent years. Light propagation and related phenomena are often simulated numerically. Due to the often required problem definition complexity these simulations typically involve methods of wave optics. Numerical simulations of light propagation through capillaries have been reported, but as a tool for flow-cell design and were limited to prediction of light path for these specific cases only [10,11].

This paper presents a developed numerical model for light propagation through multi-layered systems with cylindrical sym-metry. The model was developed to calculate light propagation and light intensity distribution within the capillaries. Macro- and micro-scale experiments were conducted to validate the model's accuracy. Such a model could be used to understand and optimise monolith synthesis within capillaries. Knowledge of light distribution within capillaries of various geometries, wall thickness, diameters and with different numbers of layers could allow for optimisation of associated regions of monolith synthesis. The presented model can also be used for designing optical detection systems and flow cells for capillary electrophoresis, liquid chromatography and flow injection analysis.

2. Experimental materials and methods

To evaluate the quality of the numerical predictions two separate sets of experiments were designed. In the first set, macro-scale experiments with cylinders of PMMA and PC were illuminated with a 532 nm wavelength green laser diode, see Fig. 2. The polymer tubes made of polymethylmetacrylate (PMMA) and polycarbonate (PC) were purchased from Access Plastic company (Dublin, Ireland). The two sets of concentric plastic cylinders were made with outer and inner diameter as follows: set A: 80 mm x 74 mm PC and 70 mm x 60 mm PMMAand set B: 80 mm x 70 mm PMMA and 70 mm x 64 mm PC. The refractive indices used in the developed models for PMMA and PC were 1.495 and 1.592 respectively [12-14].

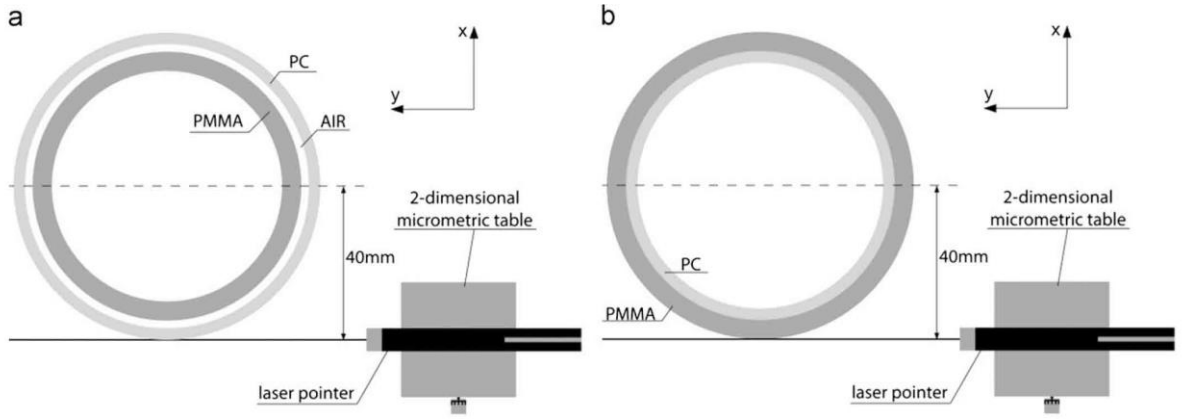

Fig. 2. Schematic plan view of initial positions of laser with (a) 80 mm × 74 mm PC and 70 mm × 60 mm PMMA concentric cylinders and the and (b) 80 mm × 70 mm PMMA and 70 mm × 64 mm PC concentric cylinders.

The macro-scale capillary experimental simulation was mounted on an optical bench. The green laser of 5 mW with wavelength of 532 nm, which was used as the light source was mounted on a micro-metric stage pointing parallel to the axis of symmetry (y-axis) as shown in Fig. 2. The laser was aligned to shine exactly along the longitudal axis of symmetry of the tube and then moved 40 mm along the x-axis such that the laser line formed a tangent to the outer cylinder. During the experiment the laser was moved by 1 mm increments toward the cylinder's centre. At each increment a picture, taken with a Panasonic LUMIX DMC-FZ30 digital camera mounted vertically overhead, was taken to measure the reflection and transmission angles in each cylinder for comparison with the corresponding numerical model results. Measurements were taken for points between 15 and 40 mm from the central axis point. These tests were repeated three times with average reflectance and transmission angles being recorded. Confidence intervals for these results using a 95% level and t-distribution were calculated.

In the second set of experiments, micro-scale experimental measurements of the optical light intensity in a 100 p.m internal diameter capillary were recorded. These measurements were com-pared with the theoretical values as determined from numerical simulations. The capillary of 1 cm length was filled with 0.01 M solution of tartrazine and illuminated with white and 430 nm violet LEDs.

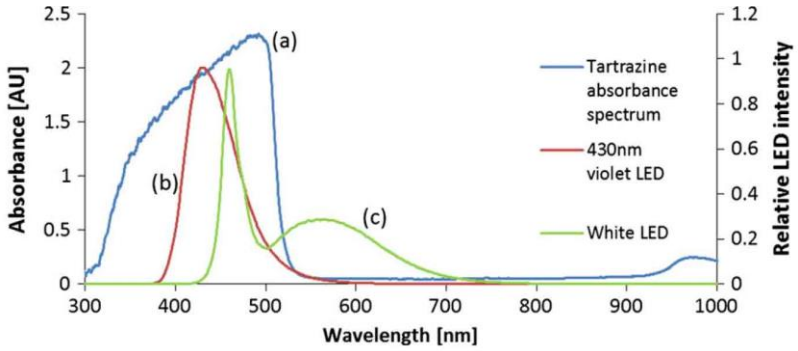

Fig. 3. (a) Measured absorbance spectrum of tartrazine, (b) relative emission spectrum of the 430 nm violet LED and (c) relative emission spectrum of the white LED.

Tartrazine is a yellow food dye with the maximum absorbance for which was measured around 425 nm, see Fig. 3. Absorbance and emissions spectra were measured using Ocean Optics MAYAProfibre optic spectrophotometer with SpectraSuiteTM software. The used Polymicro Technologies transparent PTFE coated fused silica capillaries of 100 jam internal diameter were purchased from Composite Metal Services Ltd (UK). The LED (type LED430-06) of 5 mm diameter and 430 nm central wavelength violet was purchased from RoithnerLasertechnik, GmbH, Vienna, Austria. The white LED of 5 mm diameter was manufactured by Nichia (type NSPW500GS-K1), was purchased from Dotlight, Germany. Tartrazine (CAS number 1934-21-0) was purchased from Sigma-Aldrich, Ireland.

The experimental set-up is presented in Fig. 6. Capillary pictures were taken using an Olympus BH-2 BHSP microscope fitted with a 20 x magnifying lens and an Imagingsource 1.2 megapixel USB camera. Light intensity false-colour maps were generated using Adobe® Photoshop Extended CS3 and angles were measured in scaled images processed with Image) 1.43u software. Sample statistics were calculated in IBM ii; SPSS ver. 17 statistical software package.

3. Theory and model set-up

The numerical modelling software was developed to calculate the light ray path through multi-layered cylinders, and the light intensity distribution map through the cylinder cross-sectional area. Light propagation within multimode optical fibres occurs by the phenomena of total internal reflection, where the values of refractive indices and fibre diameter remain within the limits of geometrical optics. The size of the capillary used in this work was comparable with the size of multimode optical fibres. It was assumed that capillary body, coating and bore were perfectly cylindrical and concentric. A second assumption was that the incident light had the form of parallel rays (spatially collimated), similar to laser beam light. Only the right half of the capillary cross-section is displayed in the developed model, as the diameter acts as the modelled axis of symmetry and no light ray could propagate through from left to right side. In general such occurrence is possible, but only for higher values of refractive indices approximately twice those of glass and polytetrafluor-oethylene (PTFE), which were used in this work.

The programmed model calculated the light ray path equa-tions in the Cartesian coordinate system. Separate linear functions to describe each of the light ray path segments were used (for example between air/tube, tube/tube or tube/liquid). Each light path segment was calculated in a separate subroutine calculating the light path in each zone. Incident light was in the form of rays Parallel to y-axis, see Fig. 4.

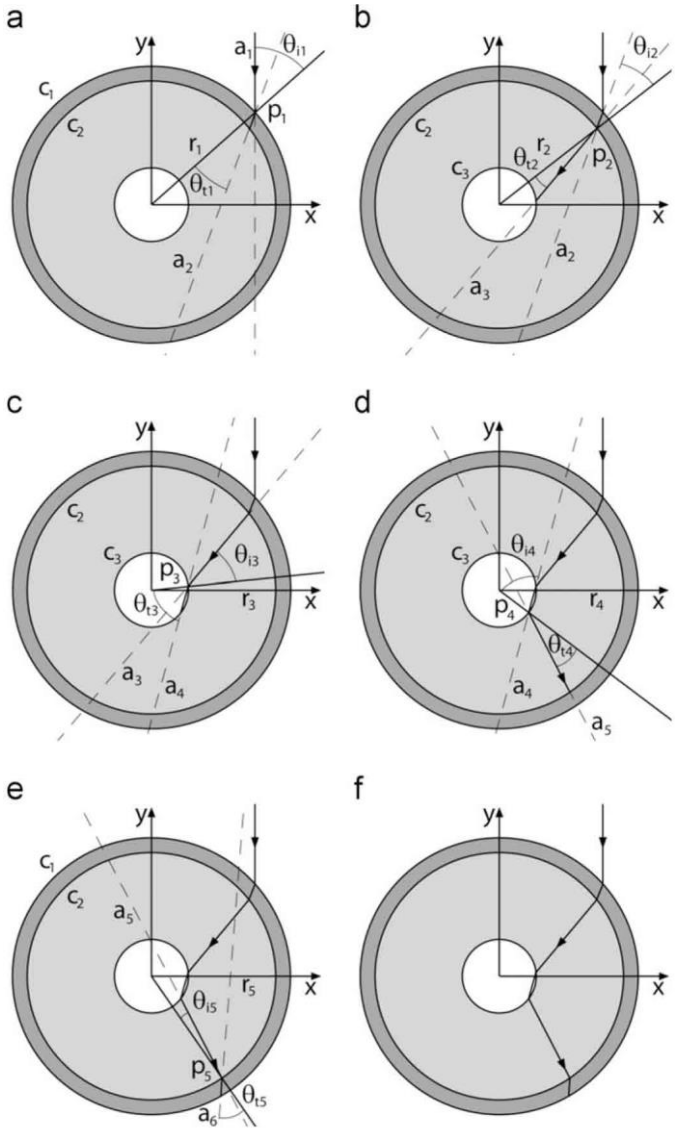

Fig. 4. (a–f) Schematic of reference lines and points, and light ray path calculated by each subroutine for light passing through a three layer system in which the light ray path is passing through a coated hollow capillary.

The first subroutine calculated the coordinates of the light incident from infinity on the air/coating boundary. This point of incidence of the ray a1 on outermost circle c_1 was assignedas $_{p1.}$ An extended radius r_1 going from(0,0) through$p_1$was drawn for calculation of angle of incidence $\theta_{il}$and in turn angle of transmission θ_{t1} was calculated from $n_i \sin\theta_i = n_t \sin\theta_t$, for the use inputted values of refractive indices n_i and n_t. A line a_2 through p_1 was drawn representing the refracted ray in the coating with θ_{t1} as the angle between a_2 and r_1,

ending the first programme subroutine, see Fig. 4a. The next subroutine began with calculation of point p_2 (where line a_2 crossed boundary c_2) and the drawing of extended radius r_2 from (0,0) through p_2. Angle of incidence θ_{i2} was calculated as the angle bounded by r_2 and a_2, see Fig. 4b. Angle of transmittance θ_{t2} was calculated from Eq. (1) and the line a_3 was drawn where $\theta_{t2}$was an angle between r_2 and a_3, ending the second programme subroutine, see Fig. 4b. This subroutine was iterated a further three times to calculate light ray paths segments along lines a_4, a_5 and a_6 after refraction on each encountered boundary. These next subroutine es of the light path formation are illustrated in Fig. 4c-e and the complete generated light path is presented in Fig. 4f without reference lines. The entire light path was represented as a sum of individual rays calculated separately according to the symbolic algorithm:

$$r = \sum_{k=1}^{2n} (a_k \cap c_k \rightarrow p_k \rightarrow r_k \rightarrow \theta_{i_k} \rightarrow \theta_{t_k} \rightarrow a_{k+1})$$

where r is the light ray path, k is the step number and n is the number of layers; a, c, p, r, θ_i and θ_t are as described earlier.

For light intensity calculations the entire capillary bore (100 μm inner diameter, which was modelled) was divided into a 0.1 μm x 0.1 μm grid and assigned with initial light intensity values of zero, see Fig. 5.

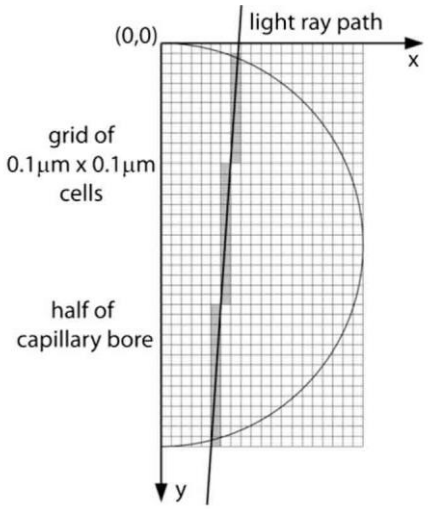

Fig. 5. Scheme of method used by algorithm for allocation of cell *x* and *y* reference values to a light ray for calculation of related light intensity values at each location.

This resolution was determined to be adequate giving 500 cells along capillary radius and 1000 cells across capillary diameter. The external capillary surface was illuminated by a set of parallel light rays spaced 0.1 µm apart. Each individual light ray was propagated through the entire capillary, giving a single light path for each incident light ray at each x-value. Modelled light ray incidence direction and x-axis direction are the same as sown in Figs. 4 and 5. Note a new origin (0,0) and y-axis direction are shown in Fig. 5. For light intensity

modelling it was assumed that there was no light absorption or attenuation in the capillary coating and capillary wall. Cell references for each light ray inside capillary bore were calculated to allow attribution of light intensity values from each ray to related cells, see Fig. 5. Along each ray path, the light intensity at each cell was calculated as a percentage of initial intensity from Eq. (2).

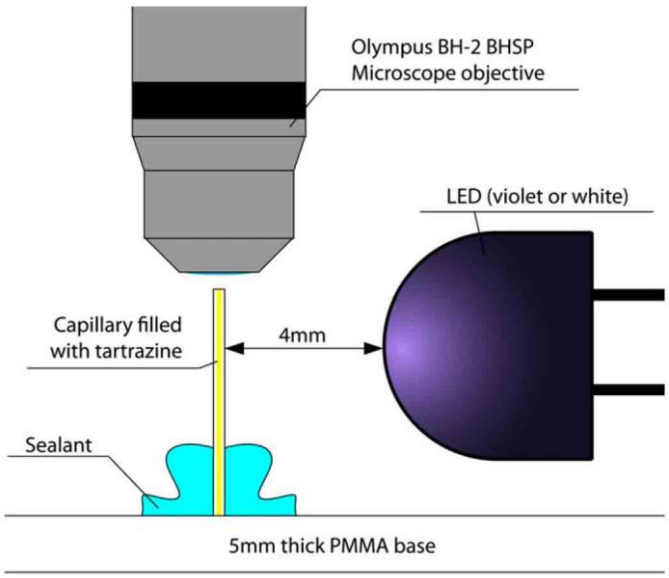

Fig. 6. Schematic of the experimental set-up for the light intensity distribution measurements inside the 100 μm inner bore capillary.

The intensity contribution from each ray to each cell was calculated separately and summed to give the total light intensity value in each cell. Due to the finite size of the cells and finite distance between incident rays, digitisation of the light intensity values across the capillary resulted. To visualise a more physically correct result all values were averaged using a 19 point moving average calculation along the x-axis. By using this 19 point moving average method, there was a loss of accurate information for a 1.9 μm region (i.e. 19 μm x 0.1 μm) at the outer diameter of the 100 μm bore (for x-values from 231 to 250). All numeric simulations were conducted on custom-built PC with the follow-ing specifications: ASUS P5E64 Workstation, INTEL $Core_2$Quad Q9450, 4GB OCZ DDR3 PC-10666, and Windows^{TM} 7 Enterprise 64 bit operating system. The ray-tracing programme was devel-oped in National Instruments LabVIEW^{TM} 9.0/2009 Service Pack 1 environment.

4. Results

4.1. Experimental and model results for first macro-simulation tests (set A)

Fig. 7 shows a picture of the laser light (532 nm) passing through the macro-experimental configuration as per experimental set A. The reflection and transmission angles (θ_{R1},$\theta_{r1}$and

θ_{r2}) presented in this picture were those selected for comparison with the numerical model results.

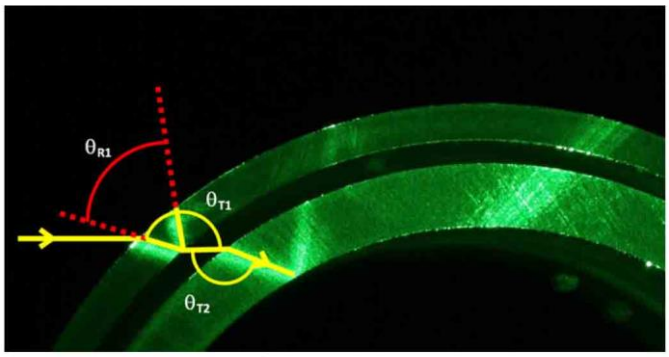

Fig. 7. Picture showing plan view of laser light passing though the outer cylinder made PC, then air and then the inner cylinder made of PMMA. The drawn solid arrow lines (green) show the laser path and construction lines (red) show the location of reflection and transmission angles (θ_{R1}, θ_{T1} and θ_{T2}). (For interpretation of the references to colour in this figure legend, the reader is referred to the web version of this article.)

The results of the angle measurements of θ_{R1},$\theta_{r1}$and $\theta_{r2}$from these experiments and the numerical models are presented in Figs. 8-10, respectively. The points in these graphs represent the average angle values for each given displacement from the centre and the whiskers on these points show the 95% confidence interval as calculated using the t-distribution. The solid line shows the corresponding results as calculated by the developed numerical based software model.

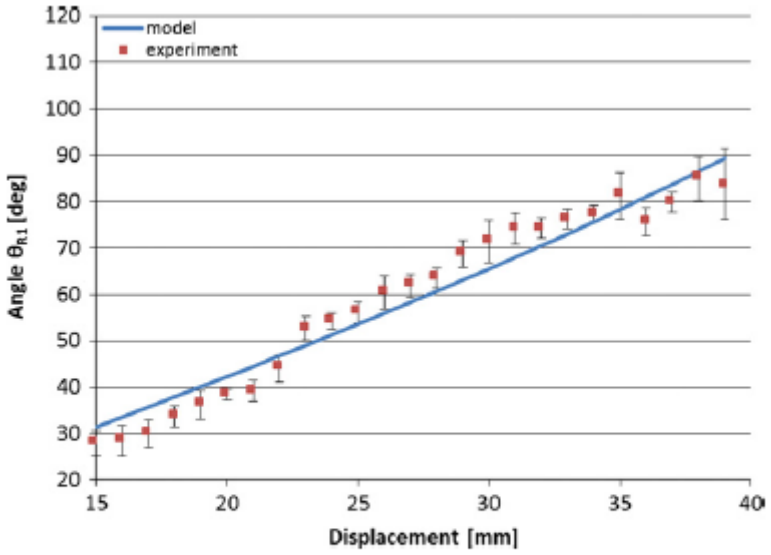

Fig. 8. Comparison of theoretical calculations from the developed software (solid blue line) with experimentally measured values for the reflection angles inside the outer cylinder (angle θ_{R1} in Fig. 10). (For interpretation of the references to colour in this figure legend, the reader is referred to the web version of this article.)

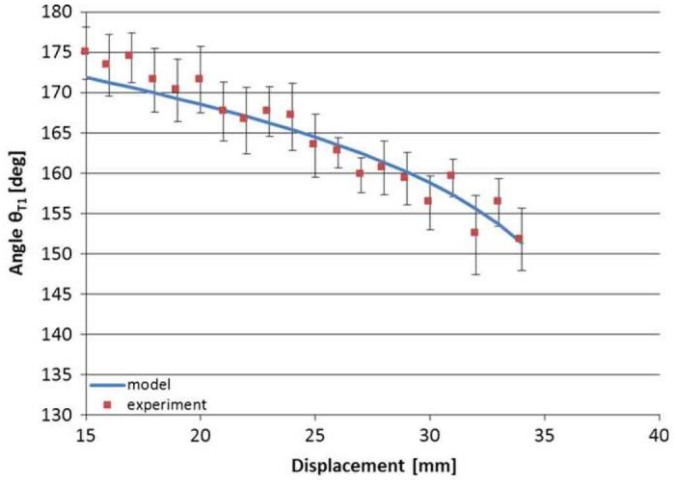

Fig. 9. Comparison of theoretical calculations from developed software (solid blue line) with experimentally measured values for the transmission angles between the first cylinder and air (angle θ_{T1} in Fig. 10). (For interpretation of the references to colour in this figure legend, the reader is referred to the web version of this article.)

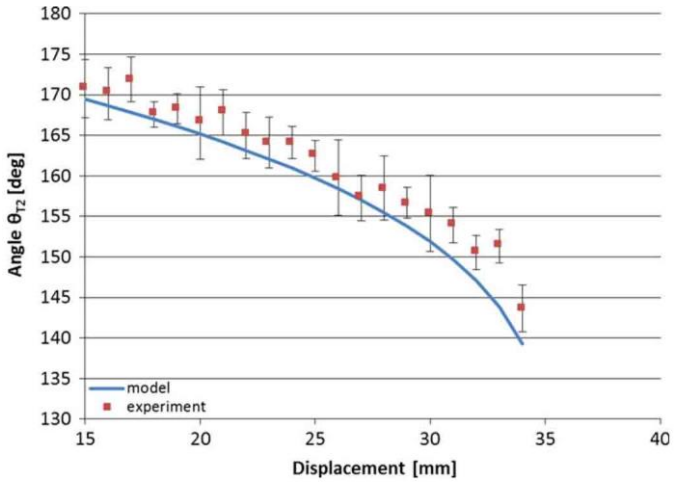

Fig. 10. Comparison of theoretical calculations from developed software (solid blue line) with experimentally measured values for the transmission angles from air to the inner cylinder (angle θ_{T2} in Fig. 10). (For interpretation of the references to colour in this figure legend, the reader is referred to the web version of this article.)

The results of the theoretical model, shown in Figs. 8-10, largely fall within the 95% confidence intervals for the experimentally measured results and follow similar trends with respect to increasing values in OR1 and reducing values of an and 0,2 for increasing displacements. These results indicated good agreement between the model and experimental measurements for testing with set A conditions, with Pearson correlation coefficients of 0.966, 0.977 and 0.986 for the angle measurements of θ_{R1}, θ_{T1} and θ_{T2}, respectively. Significance p-value (2-tailed) in all cases was below 0.001, meaning that one can reject null hypothesis and should regard data as statistically correlated and a relationship exists.

4.2. Experimental and model results for second macro-simulation tests (set B)

Fig. 11 shows a picture of the laser light (532 nm) passing through the macro-experimental configuration as per experimental set B. The reflection and transmission angles (yR1, yT1 and yT2) presented in this picture were those selected for comparison with the numerical model results. The results of the angle measurements of yR1, yT1 and yT2 from these experiments and the numerical models are presented in Figs. 12–14, respectively. The points in these graphs represent the average angle values for each given displacement from the centre and the whiskers on these points show the 95% confidence interval as calculated using the t-distribution. The solid line shows the corresponding results as calculated by the developed numerical based software model. The results of the theoretical model, shown in Figs. 12–14, largely fall outside of the 95% confidence intervals for the experimentally measured results but do, however, follow similar trends with respect to increasing values in OR, and On and reducing values of θ_rz for increasing displacements.

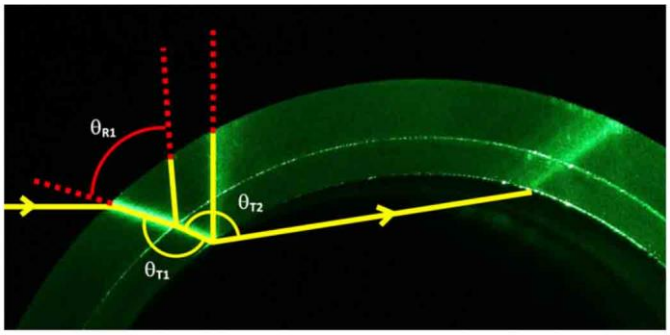

Fig. 11. Picture showing plan view of laser light passing though the outer cylinder made PMMA and then the inner cylinder made of PC. The drawn solid arrow lines (green) show the laser path and construction lines (red) show the location of reflection and transmission angles (θ_{R1}, θ_{T1} and θ_{T2}). (For interpretation of the references to colour in this figure legend, the reader is referred to the web version of this article.)

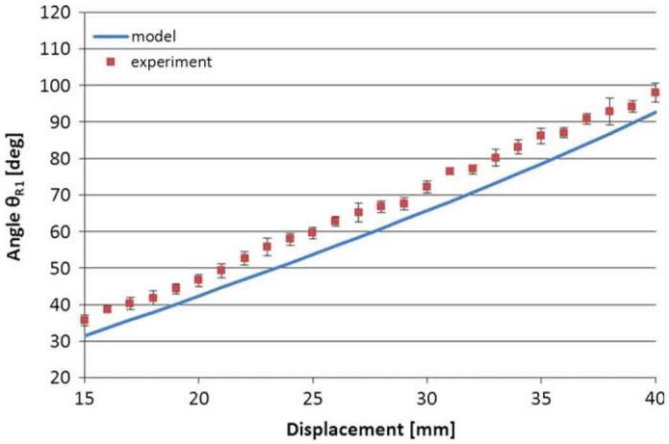

Fig. 12. Comparison of theoretical calculations from the developed software (solid blue line) with the experimentally measured values for the reflection angles inside outer cylinder (θ_{R1} angle in Fig. 14). (For interpretation of the references to colour in this figure legend, the reader is referred to the web version of this article.)

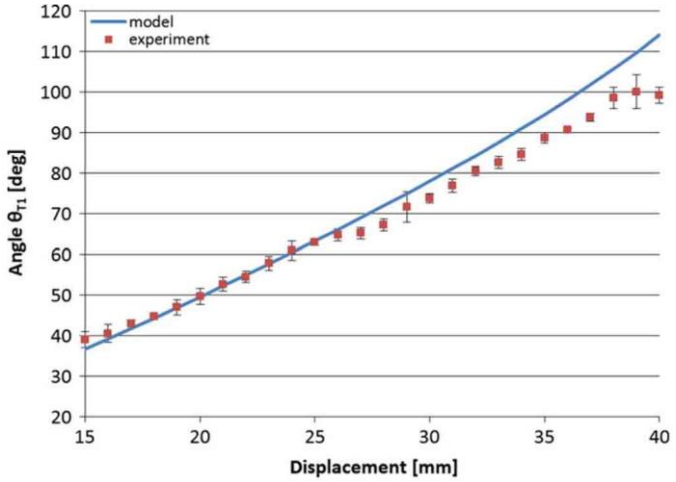

Fig. 13. Comparison of theoretical calculations from developed software (solid blue line) with experimentally measured values for the transmission angles between the cylinders (θ_{T1} angle in Fig. 14). (For interpretation of the references to colour in this figure legend, the reader is referred to the web version of this article.)

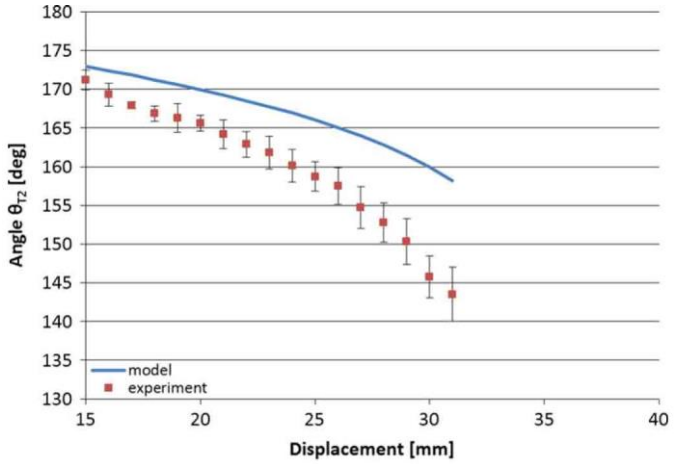

Fig. 14. Comparison of theoretical calculations from the developed software (solid blue line) with experimentally measured values for the transmission angles through air (θ_{T2} angle in Fig. 14). (For interpretation of the references to colour in this figure legend, the reader is referred to the web version of this article.)

The measured angles in Figs. 12 and 13 were, however, found to reasonably well with the theoretical predictions. Significant differences observed between modelled and measured values for θ_{rz}, see Fig. 14, are most likely due to alignment issues in the experimental set-up. These factors are considered further in the discussion section. Despite observable discrepancies between theoretical predictions and experimental results, calculated Pearson correlation coefficients were 0.997, 0.998 and 0.998 for the angle measurements of θ_{R1},$\theta_{r1}$and θ_{r2}, respectively, with significance p-value (2-tailed) below 0.001.

4.3. Experimental and model results for intensity distribution tests

Fig. 15 shows the 3D theoretically calculated light intensity distribution inside half of the 100 μm capillary filled with light absorbing solution and its 2D plan view projection. As the capillary was optically symmetrical and light ray paths could not pass from one half to the

other, only half of the capillary is shown here. The light intensity values recorded in the model were divided into six ranges as represented by the colour map shown in Fig. 15. The values from the model were scaled to fall within the range of intensity values from 135 to 255. The values shown against each colour represent the mid-point value for a range of20 on the colour intensity with values above 255 being assigned within 255-236 range.

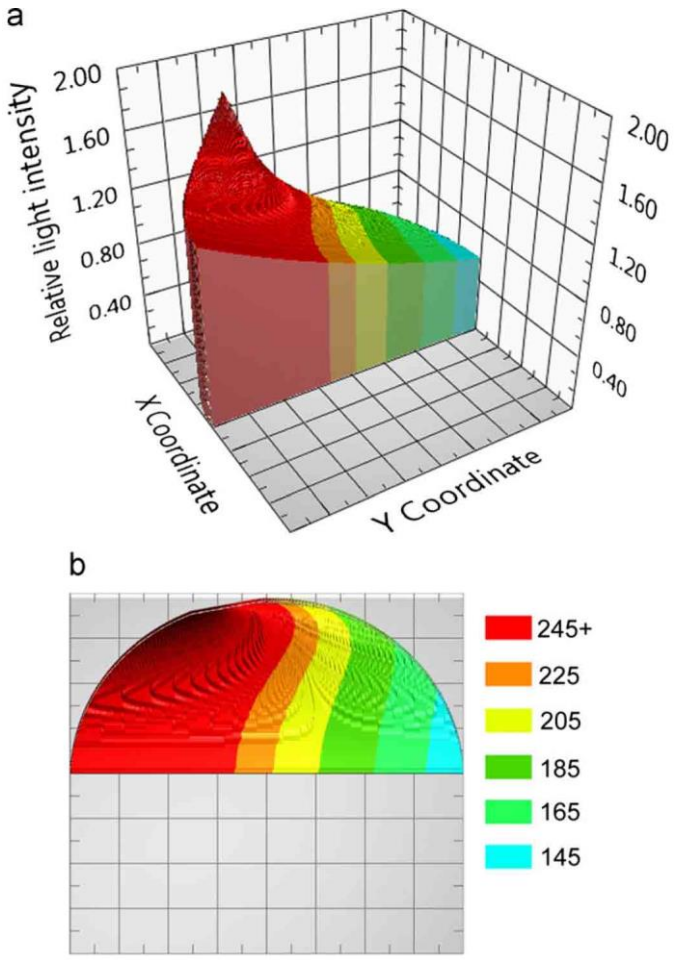

Fig. 15. (a) 3D theoretically calculated light intensity distribution inside the 100 μm inner diameter capillary filled with light absorbing solution (b) and its 2D top view projection. Light was incident along the *y*-axis (from the left side in (b)). (For interpretation of the references to colour in this figure legend, the reader is referred to the web version of this article.)

This scaling allowed for direct comparison with the experimental results shown in Fig. 16b. The range of 20 on the colour map represents a span of 7.8% in light intensity values on the scale of 0 to 255. Light was incident along the y-axis (i.e. from the left side in Fig. 15b). A series of colour photos were taken of the tartrazine filled 100 Jim inner bore diameter capillary under illumination of the LEDs. These images were saved as 256 level, grey scale, "PSD" format images. Such images directly indicate light intensity values. All pixels of intensity within a ± 10 grey scale range were selected together and a colour was assigned. For example, level 225 included all pixels within grey scale intensity level range from 216 to 235. Theoretical predic-tions were compared with these experimentally measured light intensity maps. Fig. 15a shows the photograph of the light intensity distribution inside a capillary filled

with tartrazine and illuminated with the white LED and Fig. 16b shows the same image processed into a colour map representing light intensity distribution inside the capillary. Fig. 16a shows the same capillary illuminated with the 430 nm violet LED and Fig. 16b shows the same image processed into a colour map representing light intensity distribution inside the capillary. A small shadow effect is present in the upper part of the photographs (Figs. 16a and 17a) as a result of the capillary not being perfectly cut. When com-pared to theoretical predictions, shown in Fig. 15, similar profiles can be observed.

An interesting feature clearly displayed in the theoretical model is the location of a highest intensity point at the capillary wall. Its location is a result of capillary focusing, where the capillary walls act like a lens. Although this point is not directly measured from experiment (due to a very low detector sensitivity) the layers of crescent-like distributions of the same intensity concurs well with the theoretical predictions.

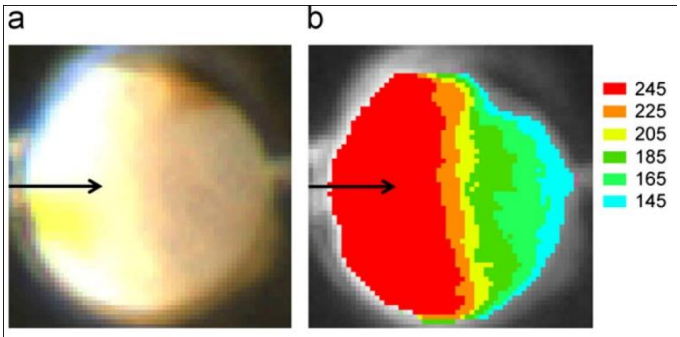

Fig. 16. (a) Capillary filled with 0.01 M tartrazine solution illuminated with white LED and (b) a colour map representing light intensity distribution inside the capillary. Arrows represent direction of illumination. (For interpretation of the references to colour in this figure legend, the reader is referred to the web version of this article.)

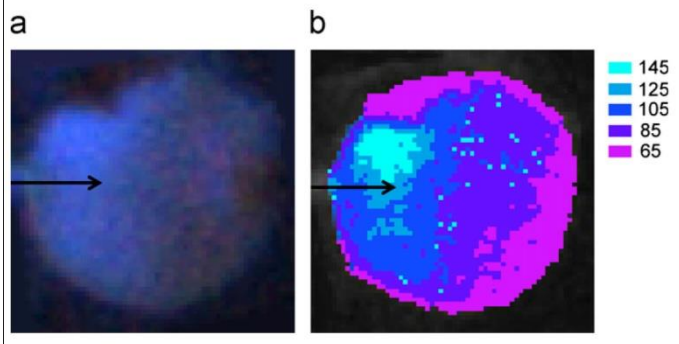

Fig. 17. (a) Capillary filled with 0.01 M tartrazine solution illuminated with 430 nm violet LED and (b) a normalised colour map representing light intensity distribution inside the capillary. Arrows represent direction of illumination. (For interpretation of the references to colour in this figure legend, the reader is referred to the web version of this article.)

5. Discussion

A numerical model of light propagation and intensity distribution for coated fused silica capillaries has been developed. Theoretical predictions of light paths are concurrent with

previous publications, and are presented with improved capability allowing taking into account the presence of coating materials and their optical proper-ties. The model itself has high flexibility allowing calculations for multiple coatings and capillary body materials with differing dimensions (coating, capillary wall thickness and bore diameters) and optical properties (refractive indices and light absorptivities). Model has been tested experimentally and showed a good agreement between theoretical predictions and measured results.

For set A macro-tests, comparison of the experimental and model results for the reflection and transmission angles (θ_{R1},$\theta_{T1}$and θ_{T2}) showed good agreement between these with model values largely lying within the 95% confidence intervals of the experimental results. The results from the models and experi-ments also trended well together. For set B macro-tests, the θ_{R1}, and θ_{T1} experimentally measured results were found to match only reasonably well with the theoretical results. These results were found to largely lie within the confidence intervals if a 2 mm additional displacement was applied to the incident light. The correlation coefficients for the set B results were higher than the values for set A indicating the closer trending of the experimental data with the model values despite higher absolute error. Reasons for observed discrepancies between theoretical and measured values are most likely due to experimental error. Much effort was invested to ensure alignment of the individual components, including mounting the experiment on an optical bench, attaching the laser on a micrometre stage, which in turn was set-up perpendicular to the edge of the cylinder's base plate, checking alignment of the reflected beams before measurement for height and perpendicularity adjustments and mounting the camera on an optical bench stand perpendicular to the top of the cylinders. However, over the scale of the experiment, alignment errors could be present due to imperfect alignment of the camera resulting in slight tilt of the incident laser beam; imperfect alignment of the laser pointer in the x-y plane resulting in a tilt of the beam; imperfect alignment of the laser pointer parallel to the x-axis of the micrometric stage; and difficulties in determination of laser beam edges in photographs resulting in inaccurate angle measurements. A slight shift and tilt of the beam from the true theoretical position could therefore be present along with some inaccurate edge detection in used image analysis routines.

From the light intensity distribution simulation an interesting focusing lens behaviour effects of the capillary were detected. The model clearly displayed the highest intensity location point at the capillary wall. These simulation results also predicted light intensities of similar magnitude in crescent-like regions emanating from the capillary walls. These distributions corresponded well with the light intensity distribution regions as measured experimentally. The shape of regions of equal intensity, their numerical values and the relative percentage changes are almost identical between the simulation and experimental results. These experimental validations show encouragingly good agreement between theoretical predictions and measured results, which could allow for optimisation of associated regions for monolith synthesis and use in fluidic chromatography, optical detection systems and flow cells for capillary electrophoresis and flow injection analysis.

References

[1] SvecF,Fre´chet JMJ.Continuous rods of macroporous polymer as high-performance liquid-chromatography separation media. AnalChem 1992; 64: 820–2.

[2]Al-BokariM,CherrakD,GuiochonG.Determination of the porosities of monolithic columnsbyinversesize-xclusionchromatography.JChromatogr A 2002;975:275–84.

[3] ViklundC,PontenE,GladB,IrgumK,HorstedtP,SvecF.‘‘Molded’’ macroporous poly (glycidylmethacrylate-co-tri methylol propane tri metha- crylate) materialswithfinecontrolledporousproperties:preparationof monoliths usingphotoinitiatedpolymerization.ChemMater1997;9:463–71.

[4] MoschouEA,NicholsonAD,JiaG,ZovalJV,MadouMJ,BachasLG,etal. Integration ofmicrocolumnsandmicrofluidicfractionatorsonmultitasking centrifugal microfluidicplatformsfortheanalysisofbiomolecules.Anal Bioanal Chem2006;285:596–605.

[5] BeilerB,SafranyA.Polymermonolithssynthesizedbyradiationco-polymer- ization insolution.RadiatPhysChem2007;76:1351–4.

[6]BandariR,KnolleW,Prager-DuschkeA,GlaselHJ,BuchmeiserMR.Monolithic media preparedviaelectronbeamcuringforproteinsseparationandflow- through catalysis.MacromolChemPhys2007;208:1428–36.

[7] WalshZ,AbeleS,LawlessB,HegerD,KlanP,BreadmoreMC,etal. Photoinitiated polymerisationofmonolithicstationaryphasesinpolyimide coated capillariesusingvisibleregionLEDs.ChemCommun2008;48: 6504–6.

[8] AbeleS,NieFQ,ForetF,PaullB,MackaM.UV-LEDphotopolymerised monoliths. Analyst2008;133:864–6.

[9] WalshZ,LevkinPA,JainV,PaullB,SvecF,MackaM.Visiblelightinitiated polymerization ofstyrenicmonolithicstationaryphasesusing470nmlight emitting diodearrays.JSepSci2010;33:61–6.

[10] BrunoAE,GassmannE,PericlesN,AntonK.On-columncapillary-flowcell utilizing opticalwave-guidesforchromatographicapplications.AnalChem 1989;61:876–83.

[11] BrunoAE,MaystreF,KrattigerB,NussbaumP,GassmannE.Thepigtailing approach tooptical-detectionincapillaryelectrophoresis.T-TrendsAnal Chem 1994;13:190–8.

[12] BrandrupJ,ImmergutEH.Polymerhandbook.JohnWiley&Sons,1975.

[13] /http://refractiveindex.info/?group=PLASTICS&material=PMMAS.

[14] /http://refractiveindex.info/?group=PLASTICS&material=PCS. T. Piaseckietal./OpticsandLasersinEngineering49(2011)924–931 931